Scientific Research Publishing

Advances in Materials Physics and Chemistry, 2024, 14, 1-14
https://www.scirp.org/journal/ampc
ISSN Online: 2162-5328
ISSN Print: 2162-531X

Investigating the Potential of Quasi-One-Dimensional Organic Crystals of $TTT(TCNQ)_2$ for Thermoelectric Applications

Silvia Andronic, Ionel Sanduleac

Department of Physics, Technical University of Moldova, Chisinau, Republic of Moldova
Email: silvia.andronic@mt.utm.md

How to cite this paper: Andronic, S. and Sanduleac, I. (2024) Investigating the Potential of Quasi-One-Dimensional Organic Crystals of $TTT(TCNQ)_2$ for Thermoelectric Applications. *Advances in Materials Physics and Chemistry*, **14**, 1-14.
https://doi.org/10.4236/ampc.2024.141001

Received: December 15, 2023
Accepted: January 23, 2024
Published: January 26, 2024

Abstract

The purpose of this paper is to present the results of investigations on quasi-one-dimensional organic crystals of tetrathiotetracene-tetracyanoquinodimethane ($TTT(TCNQ)_2$) from the prospective of thermoelectric applications. The calculations were performed after analytical expressions, obtained in the frame of a physical model, more detailed than the model presented earlier by authors. The main Hamiltonian of the model includes the electronic and phonon part, electron-phonon interactions and the impurity scattering term. In order to estimate the electric charge transport between the molecular chains, the physical model was upgraded to the so-called three-dimensional (3D) physical model. Numeric computations were performed to determine the electrical conductivity, Seebeck coefficient, thermal conductivity, thermoelectric power factor and thermoelectric figure-of-merit as a function on charge carrier concentrations, temperatures and impurity concentrations. A detailed analysis of charge-lattice interaction, consisting of the exploration of the Peierls structural transition in TCNQ molecular chains of $TTT(TCNQ)_2$ was performed. As result, the critical transition temperature was determined. The dispersion of renormalized phonons was examined in detail.

Keywords

Organic Materials, Tetrathiotetracene-Tetracyanoquinodimethane, Thermoelectric Figure of Merit, Renormalized Phonon Spectrum, Peierls Transition

1. Introduction

Energy plays a crucial role in both industrial processes and daily life. Currently,

around 90% of the world's annual energy consumption, which is approximately 15 terawatt-years, is derived from heat engines fueled by fossil sources. However, these engines operate at a modest efficiency of 30% - 40%, resulting in a substantial amount of heat being dissipated into the environment. It is important to find cost-effective technologies for 2 generating electricity from even a part of this waste heat. Thermoelectric generators are anticipated to play a key role in achieving this objective. Additionally, these generators can function as refrigerators, directly converting electrical energy into cold without the need for a compressor.

The primary factor influencing a material's viability for use in thermoelectric energy converters is the dimensionless thermoelectric figure of merit, denoted as $ZT = \sigma S^2 T/k$. Here, σ represents electrical conductivity, S denotes thermopower (Seebeck coefficient), $k = k^e + k^L$ is the thermal conductivity, which consists from electronic k^e and phononic k^L contributions and T is the operating temperature. The goal is to achieve the highest possible ZT values. While it might seem intuitive to increase σ and S while decreasing k simultaneously, these parameters are independent. Enhancing σ may reduce S and increase k^e, and vice versa. Despite this, significant progress in the increase of ZT has been made in recent decades, particularly in low-dimensional inorganic structures. Remarkable ZT values, such as ~2.4 has been measured [1] at room temperature in p-type Bi_2Te_3/Sb_2Te_3 superlattices. $ZT \sim 3$ has been reported in PbTeSe quantum dot superlattices [2], and even $ZT \sim 3.5$ [3] [4] have been reported. However, these achievements involve technologically complex and costly structures. Although the current commercially used thermoelectric materials based on Bi_2Te_3 have $ZT \sim 1$ around 500 K, this is considered relatively low. Attaining $ZT > 3$ would make solid-state converters economically competitive with conventional alternatives, but commercialization is currently limited. Nevertheless, there are instances of mass-producing miniature thermoelectric modules for applications such as maintaining constant temperatures in laser diodes [5], climate control seats in hundreds of thousands of vehicles annually [6], portable beverage coolers [7], and various other uses, including space applications. In [8] a comprehensive review was conducted on thermoelectric materials and their applications. A prospective strategy for scaling up the production of miniaturized thermoelectric devices is suggested, involving the integration of high-energy ball milling and aerosol jet printing. High ZT values are achieved through a combination of high electrical conductivity and low thermal conductivity values [9] [10] [11].

In recent years, there has been a growing focus on organic compounds, capturing the attention of researchers. These materials are not only cost-effective and abundant but also exhibit diverse and often unconventional properties when compared to their inorganic counterparts. Additionally, they have the advantage of being environmentally friendly. One notable example is poly(3,4-ethylenedioxythiophene) (PEDOT) doped with poly(styrenesulphonate) (PSS), where thin films of p-type have registered a ZT value of 0.42 at room temperature [12]. For n-type materials, the most promising result has been achieved with powder-processed inorganic hybrid polymer, poly[Kx-(Ni-ett)], with a ZT value of 0.2 at

400 K [13]. Furthermore, even higher ZT values, reaching around 1, have been reported in films of PP-PEDOT/Tos [14]. This underscores the potential of organic compounds in advancing thermoelectric technology.

We have anticipated substantial ZT values in certain quasi-one-dimensional (Q1D) organic crystals, including TTT_2I_3 [15] and $TTT(TCNQ)_2$ [16]. Organic crystals with a Q1D structure are composed of linear chains or stacks of molecules arranged in a three-dimensional crystal lattice. Many organic materials exhibit quasi-one-dimensional structure, such as ion-radical salts like tetrathiofulvalene-tetracyanoquinodimethane (TTF-TCNQ), crystal polymers, and specific charge transfer complexes. In Q1D crystals, the interaction between molecules along the chains is more pronounced than between different chains, resulting in needle-like shapes and often unique properties. Previous predictions of high ZT values in Q1D organic crystals were based on a simplified strictly 1D physical model. We have developed a more realistic 3D model, enabling a more precise simulation of the thermoelectric properties of select Q1D organic crystals.

The aim of this paper is to present the findings from investigations conducted in recent years, focusing on Q1D organic crystals for potential applications in thermoelectric systems. The research involves a comprehensive examination, modeling, and analysis of various properties such as electrical conductivity, Seebeck coefficient, thermal conductivity, thermoelectric power factor and the thermoelectric figure of merit within these crystals. Furthermore, the study explores the Peierls structural transition in TCNQ molecular chains of $TTT(TCNQ)_2$, determining the critical transition temperature and analyzing the dispersion of renormalized phonons at different temperatures and various dimensionless Fermi momentum (k_F) values. The paper is structured as follows. Section 2 describes three-dimensional model of the crystal. Section 3 presents the results of computer simulations. The conclusions are formulated in Section 4.

2. The Physical Model in 3D Approximation for $TTT(TCNQ)_2$

In this Section we will present the physical model of the $TTT(TCNQ)_2$ crystal. The Hamiltonian of the 3D crystal model, employing tight binding and nearest neighbor approximations, is expressed in the following form:

$$H = \sum_{\boldsymbol{k}} \varepsilon(\boldsymbol{k}) a_{\boldsymbol{k}}^{+} a_{\boldsymbol{k}} + \sum_{\boldsymbol{q}} \hbar\omega_{\boldsymbol{q}} b_{\boldsymbol{q}}^{+} b_{\boldsymbol{q}} + \sum_{\boldsymbol{k},\boldsymbol{q}} A(\boldsymbol{k},\boldsymbol{q}) a_{\boldsymbol{k}}^{+} a_{\boldsymbol{k}-\boldsymbol{q}} \left(b_{\boldsymbol{q}} + b_{-\boldsymbol{q}}^{+}\right). \quad (1)$$

Let's describe each component of Equation (1). The first term corresponds to the energy operator of free electrons within the periodic field of the lattice. The second term represents the energy operator of longitudinal acoustic phonons. The third term characterizes the interactions between electrons and phonons. Here, $\varepsilon(\boldsymbol{k})$ denotes the energy of the carrier, where a_k^+ and a_k are the creation and annihilation operators of the electron with a 3D quasi-wave vector $\boldsymbol{k}$ and projections (k_x, k_y, k_z). Similarly, b_q^+ and b_q represent the creation and annihilation operators of an acoustic phonon with a 3D wave vector $\boldsymbol{q}$ and frequency ω_q. $A(\boldsymbol{k},\boldsymbol{q})$ represents the matrix element of interaction. The energy

of the electron, $\varepsilon(\boldsymbol{k})$ is measured from the band top, and this term is presented in the following form:

$$\varepsilon(\boldsymbol{k}) = 2w_1(1-\cos k_x b) - 2w_2(1-\cos k_y a) - 2w_3(1-\cos k_z c). \quad (2)$$

Here, w_1, w_2, and w_3 represent the transfer energies of an electron from the specified molecule to its nearest neighbors along the lattice vectors $\boldsymbol{b}$, $\boldsymbol{a}$, and $\boldsymbol{c}$. The coordinate axes x, y, z align with $\boldsymbol{b}$, $\boldsymbol{a}$, and $\boldsymbol{c}$ respectively, and the conductive chains are oriented along $\boldsymbol{b}$. The quasi-one-dimensionality assumption implies that w_1 is significantly larger than w_2 and w_3.

Only longitudinal acoustic phonons are considered due to their significance as the primary scattering mechanism. The dispersion law is as follows:

$$\omega_{\boldsymbol{q}}^2 = \omega_1^2 \sin^2(bq_x/2) + \omega_2^2 \sin^2(aq_y/2) + \omega_3^2 \sin^2(cq_z/2), \quad (3)$$

where ω_1, ω_2 and ω_3 are limit frequencies in the x, y and z directions, $\boldsymbol{q}$ is a phonon quasi-wave vector with the projections (q_x, q_y, q_z). Due to the same quasi-one-dimensionality, ω_1 is much bigger than ω_2 and ω_3.

Two the most important interactions of electrons with acoustic phonons are considered, generalized for the 3D case. One of them is of deformation potential type. Three coupling constants of this mechanism are proportional to the derivatives w_1', w_2' and w_3' with respect to the intermolecular distance of w_1, w_2, and w_3. The other interaction is similar to that of polaron. The coupling constant is proportional to the mean polarizability of the molecule α_0. The square of absolute module of the hole-phonon interaction $A(\boldsymbol{k},\boldsymbol{q})$ which appear in the expression of scattering probability has the form

$$\begin{aligned} |A(\boldsymbol{k},\boldsymbol{q})|^2 = 2\hbar/(NM\omega_q)\{ & w_1'^2[\sin(k_x b) - \sin((k_x - q_x)b) + \gamma_1 \sin(q_x b)]^2 \\ & + w_2'^2[\sin(k_y a) - \sin((k_y - q_y)a) + \gamma_2 \sin(q_y a)]^2 \\ & + w_3'^2[\sin(k_z c) - \sin((k_z - q_z)c) + \gamma_3 \sin(q_z c)]^2\} \end{aligned} \quad (4)$$

Here, M represents the mass of the TTT molecule, and N is the count of molecules in the crystal's fundamental region. The parameters γ_1, γ_2 and γ_3 signify the ratios of amplitudes for the second interaction compared to the first one in the direction of chains and in transversal directions. These parameters can be determined using the expressions provided below

$$\gamma_1 = 2e^2\alpha_0/b^5 w_1', \quad \gamma_2 = 2e^2\alpha_0/a^5 w_2', \quad \gamma_3 = 2e^2\alpha_0/c^5 w_3'. \quad (5)$$

The analysis includes hole scatterings on point-like and neutral impurities, as well as on static and thermally activated defects. The description of these scattering rates at room temperature involves a dimensionless parameter, denoted as D_0, which can be minimized significantly under conditions of high crystal purity and perfection.

Applying the theory of linear nonreversible processes, we can express the electrical conductivity through the two particle retarded Green function. The chain of equations for the two particle Green function is decoupled by expressing the

three particle Green Functions through the two particle ones. As result we obtain a closed equation for the two particle Green function, which can be solved and expressed through the mass operator M_k^x of the two particle Green function, defined in the form

$$M_{\boldsymbol{k}}^x = \sum_{\boldsymbol{q}} W_{\boldsymbol{k}+\boldsymbol{q},\boldsymbol{k}} \left[1 - \frac{v_x(\boldsymbol{k}+\boldsymbol{q})}{v_x(\boldsymbol{k})} \right], \tag{6}$$

where $W_{k+q,k}$ is the electron-phonon scattering probability.

$$\begin{aligned} W_{\boldsymbol{k}+\boldsymbol{q},\boldsymbol{k}} = 2\pi\hbar^{-1} \left| A(\boldsymbol{k}+\boldsymbol{q},\boldsymbol{q}) \right|^2 \left\{ \left(1+N_{\boldsymbol{q}}-n_{\boldsymbol{k}+\boldsymbol{q}}\right) \delta\left[E(\boldsymbol{k}+\boldsymbol{q}) - E(\boldsymbol{k}) + \hbar\omega_{\boldsymbol{q}} \right] \right. \\ \left. + \left(N_{\boldsymbol{q}}+n_{\boldsymbol{k}-\boldsymbol{q}}\right) \delta\left[E(\boldsymbol{k}+\boldsymbol{q}) - E(\boldsymbol{k}) - \hbar\omega_{\boldsymbol{q}} \right] \right\} \end{aligned} \tag{7}$$

Here N_q is the phonon distribution function. When an electric field and a temperature gradient are applied in x direction along chains and the electrical and thermal flows are calculated in the x direction too, we obtain for the electrical conductivity, σ_{xx} thermopower S_{xx}, electronic thermal conductivity k_{xx}^e and thermoelectric figure of merit $(ZT)_{xx}$ the expressions

$$\sigma_{xx} = \frac{e^2}{k_B T V} \sum_{\boldsymbol{k},\sigma} \frac{v_x^2(\boldsymbol{k}) n_{\boldsymbol{k}} (1-n_{\boldsymbol{k}})}{M_{\boldsymbol{k}}^x}, \tag{8}$$

$$S_{xx} = -\frac{1}{eT} \sum_{\boldsymbol{k},\sigma} \frac{\left[E(\boldsymbol{k}) - E_F \right] v_x^2(\boldsymbol{k}) n_{\boldsymbol{k}} (1-n_{\boldsymbol{k}})}{M_{\boldsymbol{k}}^x} \Bigg/ \sum_{\boldsymbol{k},\sigma} \frac{v_x^2(\boldsymbol{k}) n_{\boldsymbol{k}} (1-n_{\boldsymbol{k}})}{M_{\boldsymbol{k}}^x}, \tag{9}$$

$$\begin{aligned} k_{xx}^e = \frac{1}{k_B T^2 V} \left\{ \sum_{\boldsymbol{k},\sigma} \frac{\left[E(\boldsymbol{k}) - E_F \right]^2 v_x^2(\boldsymbol{k}) n_{\boldsymbol{k}} (1-n_{\boldsymbol{k}})}{M_{\boldsymbol{k}}^x} \right. \\ \left. - \left[\sum_{\boldsymbol{k},\sigma} \frac{\left[E(\boldsymbol{k}) - E_F \right] v_x^2(\boldsymbol{k}) n_{\boldsymbol{k}} (1-n_{\boldsymbol{k}})}{M_{\boldsymbol{k}}^x} \right]^2 \Bigg/ \sum_{\boldsymbol{k},\sigma} \frac{v_x^2(\boldsymbol{k}) n_{\boldsymbol{k}} (1-n_{\boldsymbol{k}})}{M_{\boldsymbol{k}}^x} \right\}, \end{aligned} \tag{10}$$

$$ZT_{xx} = \sigma_{xx} S_{xx}^2 T \Big/ \left(k_{xx}^L + k_{xx}^e \right), \tag{11}$$

where V represents the volume of the crystal's fundamental region, $v_x(\boldsymbol{k})$ denotes the projection of carrier velocity on x direction, e is the carrier charge, k_B is the Boltzmann constant, n_k is the Fermi distribution function, k_{xx}^L represents the lattice thermal conductivity. At room temperature, we can consider the electron-phonon scattering processes elastic and we can also neglect the transversal kinetic energy of the carrier in Equation (7). Then integration in Equation (6) on the whole Brillouin zone can be realized analytically and finally we obtain

$$\begin{aligned} M_{\boldsymbol{k}}^x = \frac{4b^2 k_B T (w_1')^2}{v_{s1}^2 \hbar m \left| w_1 \sin(k_x b) \right|} \left\{ \left[1 - \gamma_1 \cos(k_x b) \right]^2 \right. \\ + \frac{d_1}{8\sin^2(k_x b)} \left[1 + 2\sin^2(k_y a) - 2\gamma_2 \cos(k_y a) + \gamma_2^2 \right] \\ \left. + \frac{d_2}{8\sin^2(k_x b)} \left[1 + 2\sin^2(k_z c) - 2\gamma_3 \cos(k_z c) + \gamma_3^2 \right] + D_0 \right\} \end{aligned} \tag{12}$$

where v_{s1} is the sound velocity along chains, $d_1 = w_2/w_1 = w_2'/w_1'$,

$d_2 = w_3/w_1 = w_3'/w_1'$, D_0 describes the electron scattering rate on impurities, on static and thermally activated defects at room T.

To determine the parameters d_1 and d_2, we have calculated the electrical conductivity in the transversal directions, namely σ_{yy} and σ_{zz}. Along these axes, the overlap of electron wave functions is minimal, making it more practical to express the system's Hamiltonian in the localized states representation. Specifically for the y and z directions, the dominant term in the Hamiltonian is the electron-phonon interaction, while the component describing electron motion in the periodic lattice potential is treated as a small perturbation. Consequently, a canonical transformation is applied to the Hamiltonian, allowing us to account for the primary part of the electron-phonon interaction in the zero approximation. This results in a significant narrowing of the initial conduction band along the conductive chains. As a result, transport in the transversal directions adopts a hopping-type nature, with carriers manifesting as small polarons.

Expressions for σ_{yy} and σ_{zz} were calculated numerically. By comparing them with the experimental data of $\sigma_{yy} \sim \sigma_{zz} = 3.3$ $\Omega^{-1}\cdot\text{cm}^{-1}$, it can be estimated that $w_2 = w_3 = 0.015 w_1$. These values are of the same order because the lattice constants a and c in y and z direction are very close to each other.

The investigation delves into the Peierls structural transition within TCNQ molecular chains of $TTT(TCNQ)_2$. A more complete physical model of the crystal is applied, that consider simultaneously two the most important electron-phonon interactions mentioned higher. The analytic expressions for the phonon Green function and for the phonon polarization operator are obtained in the random phase approximation. The effects of interchain interaction on the phonon dispersion and on Peierls critical temperature are estimated. The effects of interchain interaction on the dispersion of renormalized phonons and on Peierls critical temperature for different values of Fermi dimensionless quasi momentum are analyzed. In order to deduce the expression for renormalized phonon Green function we apply the random phase approximation. From exact series of perturbation theory for the phonon Green function we sum up the diagrams containing 0, 1, 2, …, ∞ closed loops of two electron Green functions that make the most important contribution. We obtain for the Fourier component of the phonon Green function $D(\boldsymbol{q},\Omega)$:

$$D(\boldsymbol{q},\Omega) = D_0(\boldsymbol{q},\Omega) - D_0(\boldsymbol{q},\Omega)\Pi(\boldsymbol{q},\Omega)D(\boldsymbol{q},\Omega) \tag{13}$$

where $D_0(\boldsymbol{q},\Omega)$ is the phonon polarization operator, $D_0(\boldsymbol{q},\Omega)$ is the free phonon Green function, $\boldsymbol{q}$ is the wave vector of longitudinal acoustic phonons and $\Omega(\boldsymbol{q})$ is the renormalized phonon frequency. The real part of the dimensionless polarization operator is presented in the form:

$$\text{Re}\,\overline{\Pi}(\boldsymbol{q},\Omega) = -\frac{\overline{N}}{2\pi^3\hbar\omega_{\boldsymbol{q}}}\int_{-\pi}^{\pi}\mathrm{d}k_x\int_{-\pi}^{\pi}\mathrm{d}k_y\int_{-\pi}^{\pi}\mathrm{d}k_z\left|A(\boldsymbol{k},\boldsymbol{q})\right|^2 \times \frac{n_{\boldsymbol{k}} - n_{\boldsymbol{k}+\boldsymbol{q}}}{\varepsilon(\boldsymbol{k}) - \varepsilon(\boldsymbol{k}+\boldsymbol{q}) + \hbar\Omega} \tag{14}$$

In Equation (14) $\overline{N}$ represents the number of elementary cells in the basic region of the crystal, where $N = r\overline{N}$, with r being the number of molecules in

the elementary cell ($r = 2$), $A(\boldsymbol{k},\boldsymbol{q})$ signifies the matrix element of electron-phonon interaction presented in Equation (4), $\varepsilon(\boldsymbol{k})$ denotes the carrier energy, $\hbar$ is the Planck constant, n_k is the Fermi distribution function. The renormalized acoustic phonons spectrum $\Omega(\boldsymbol{q})$ is determined by the pole of function $D(\boldsymbol{q},\Omega)$ and is obtained from the transcendent dispersion equation

$$\Omega(\boldsymbol{q}) = \omega_{\boldsymbol{q}}\left[1-\overline{\Pi}(\boldsymbol{q},\Omega)\right]^{1/2} \tag{15}$$

Equation (15) can be solved only numerically.

3. Results and Discussions

Crystals of $TTT(TCNQ)_2$ can be obtained by simple chemical methods in form of dark-violet needles of length 3 - 6 mm [17]. This compound, characterized as a charge-transfer complex, consists of chains of TTT anions and TCNQ cations. The internal structure exhibits pronounced quasi-one-dimensionality, with lattice constants c = 3.75 Å, b = 12.97 Å, and a = 19.15 Å along the x, y, and z directions, respectively [17]. It's noteworthy that the x-axis aligns parallel to TCNQ chains along c. The primary charge transport occurs along TCNQ chains, with an electron transfer energy of $w_1 = 0.125$ eV between nearest TCNQ molecules in the x direction. In transversal directions, the parameters $w_2 = d_1 \cdot w_1$ and $w_3 = d_2 \cdot w_1$ are relatively small, indicating a hopping-type transport mechanism. The parameters d_1 and d_2 have the values of $d_1 = 0.015$ and $d_2 = 0.015$ for $TTT(TCNQ)_2$. The sound velocity was estimated by modeling of Peierls structural transition, $v_{s1} \approx 4\times10^3$ m/s. In transversal directions, $v_{s2} \approx v_{s3} = v_{s1}/2$. Additionally, γ_1 is estimated to be 1.7. The stoichiometric electron concentration in $TTT(TCNQ)_2$ crystals is approximately $n = 1.1\times10^{21}$ cm^{-3} or $\varepsilon_F = 2w_1/E_F = 0.35$, where E_F represents the Fermi energy, and ε_F is the dimensionless Fermi energy. The mass of a TCNQ molecule is $M = 3.72\times10^5 m_e$, where m_e is the mass of a free electron. The number of molecular chains per elementary cell is $r = 2$.

Thermoelectric properties are modeled numerically as function of dimensionless Fermi energy for crystals with different purity.

In **Figure 1**, the electrical conductivity along the TCNQ chains at room temperature is presented. For stoichiometric crystals, σ_{xx} is low (~10^3 $\Omega^{-1}\cdot cm^{-1}$) and the difference between 3D and 1D physical models is not distinguishable. It is observed that the increase of ε_F leads to a significant increase of σ_{xx}, which achieves values up to 13.5 × 10^3 $\Omega^{-1}\cdot cm^{-1}$ for the purest crystals with $D_0 = 0.02$, if the concentration on conducting electrons is doubled with respect to the stoichiometric value ($n = 2.2\times10^{21}$ cm^3 or $\varepsilon_F = 1.05$). From the behavior of electrical conductivity, it can be observed that, the higher the purity of the crystal, the more evident becomes the interchain interaction and the deviation of the 3D model from the 1D increases.

For stoichiometric crystals S_{xx} ~ −120 μV/K (**Figure 2**), and this value is practically independent of crystal purity. If ε_F is increased, the absolute value of thermopower first decreases, reaching a maximum value and decreases again to

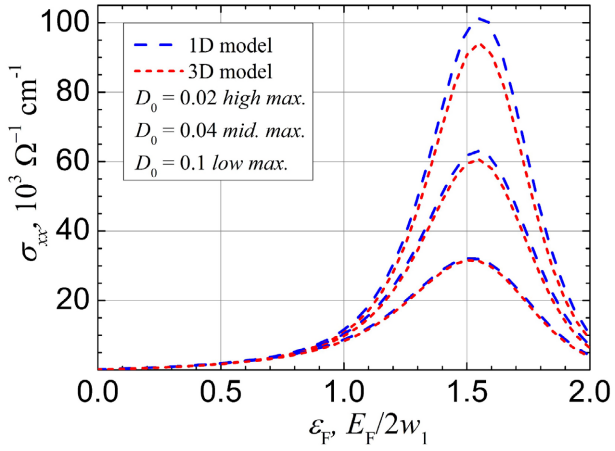

Figure 1. Electrical conductivity σ_{xx} along TCNQ chains as function of E_F.

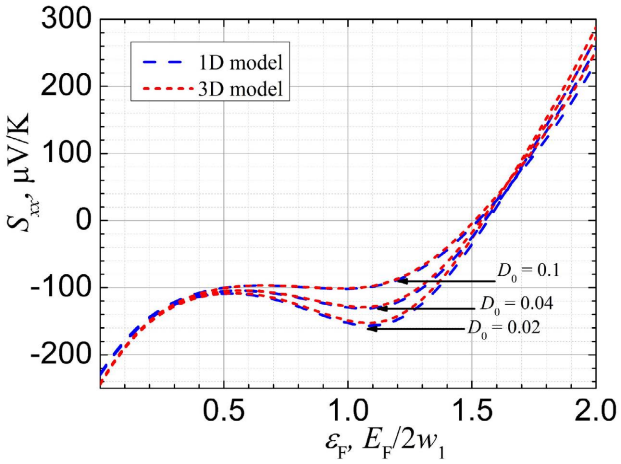

Figure 2. Seebeck coefficient S_{xx} along TCNQ chains as function of Fermi energy E_F.

zero. The region with positive S_{xx} indicates that for $\varepsilon_F > 1.05$ the charge carriers become holes. If the concentration of electrons in increased twofold, $n = 2.2\times10^{21}$ cm^3 or $\varepsilon_F = 1.05$, S_{xx} = −100, −130 and −152 μV/K for crystals with $D_0 = 0.1, 0.04, 0.02$. This is a very promising result, leading to the increase of the power factor (**Figure 3**).

Purification of the crystals ensure an additional increase of the power factor, up to 17 × 10^{-3} W·m^{-1}·K^{-2} (~4 times higher than for Bi_2Te_3) and even 31.2 × 10^{-3} W·m^{-1}·K^{-2} for the purest crystals with $D_0 = 0.02$.

For $\varepsilon_F = 1.05$ the thermal conductivity (**Figure 4**) is provided mainly by the electrons, $k_{xx}^e \sim 13.2$ W·m^{-1}·K^{-1}, while the lattice contribution is only 0.4 W·m^{-1}·K^{-1}. It is observed that the maxima of k_{xx}^e are slightly displaced toward lower ε_F in comparison with the maxima of σ_{xx}. This phenomenon reveals the violation of the Wiedemann-Franz law.

Thermoelectric figure of merit (**Figure 5**) in stoichiometric crystals is small, $(ZT)_{xx}$ ~ 0.05, and remains small, even if the crystal is strongly purified. This takes place because the electronic thermal conductivity and electrical conductiv-

ity increases simultaneously. If the concentration of conducting electrons is two-fold increased with respect to the stoichiometric one ($n = 2.2 \times 10^{21}$ cm^3 or $\varepsilon_F = 1.05$), $(ZT)_{xx}$ = 0.07, 0.23 and 0.35 for crystals with $D_0 = 0.6, 0.2, 0.1$ and $(ZT)_{xx}$ = 0.53, 0.68 for crystals with $D_0 = 0.04, 0.02$. If ε_F is increased up to 1.2, a value of $(ZT)_{xx}$ near unity is predicted.

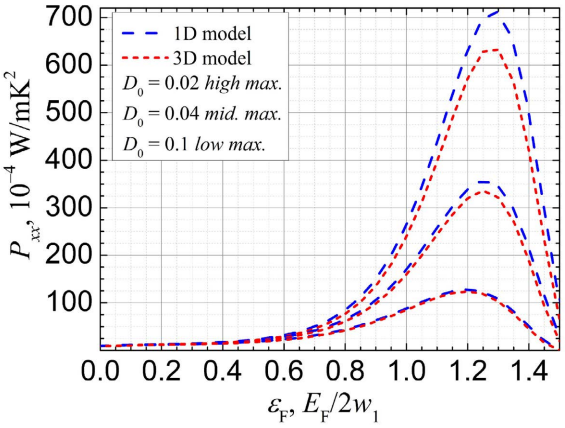

Figure 3. Power factor P_{xx} along TCNQ chains as function of E_F.

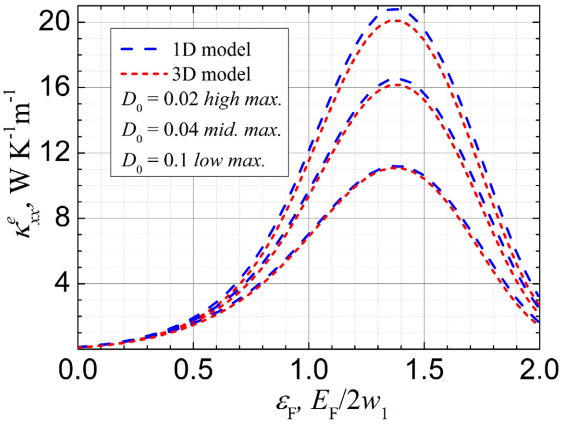

Figure 4. Electronic thermal conductivity k^e_{xx} along TCNQ chains as function of E_F.

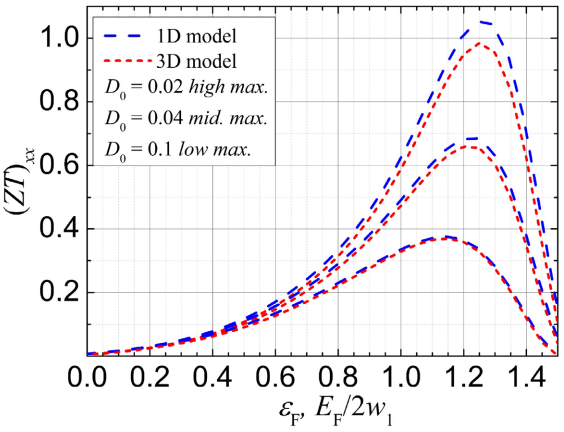

Figure 5. Thermoelectric figure of merit $(ZT)_{xx}$ along TCNQ chains as function of E_F.

In the following we will discuss about the behavior of the Peierls transition in Q1D organic crystals of $TTT(TCNQ)_2$. The Peierls transition has been studied by many authors [18] [19]. In the previous paper it was studied the behavior of Peierls transition in TTF-TCNQ crystals [20] and in TTT_2I_3 organic materials [21]. The aim of this paper is to offer a comprehensive model of the Peierls transition in $TTT(TCNQ)_2$ crystals within the context of a complete physical model in 3D approximation, that takes into account, simultaneously, the two most significant electron-phonon interactions mentioned earlier.

In **Figures 6-9**, we illustrate the variations of renormalized phonon frequencies, denoted as $\Omega(q_x)$, with respect to q_x, considering different temperatures, q_y and q_z values, and Fermi quasi-momentum (k_F). Here, q_x, q_y and q_z represent

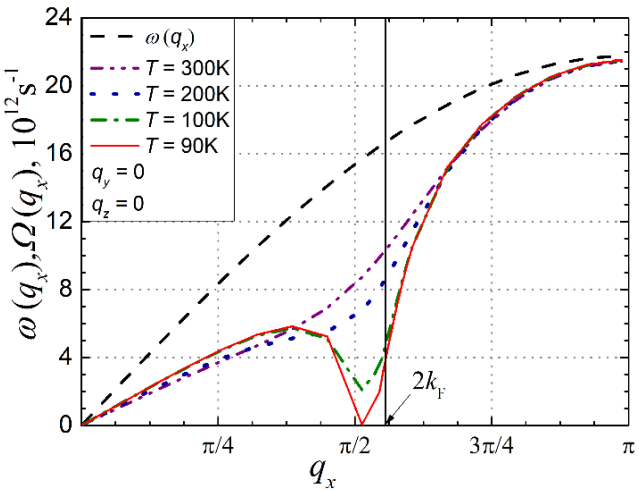

Figure 6. Renormalized phonon spectrum $\Omega(q_x)$ is plotted for various temperatures, with $\gamma_1 = 1.7$. The dashed line represents the spectrum of free phonons. Dimensionless Fermi momentum is $k_F = 0.56\pi/2$.

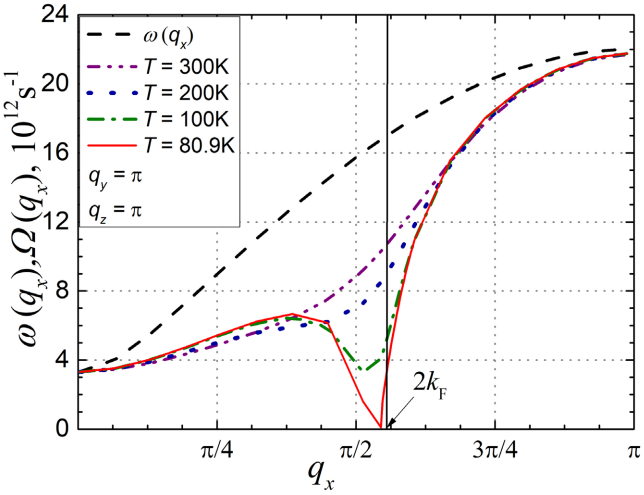

Figure 7. Renormalized phonon spectrum $\Omega(q_x)$ is plotted for various temperatures, with $\gamma_1 = 1.7$. The dashed line represents the spectrum of free phonons. Dimensionless Fermi momentum is $k_F = 0.56\pi/2$.

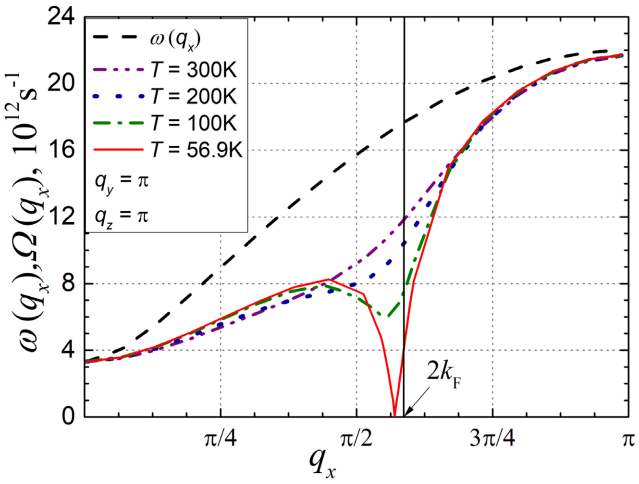

Figure 8. Renormalized phonon spectrum $\Omega(q_x)$ is plotted for various temperatures, with γ_1 = 1.7. The dashed line represents the spectrum of free phonons. Dimensionless Fermi momentum is $k_F = 0.59\pi/2$.

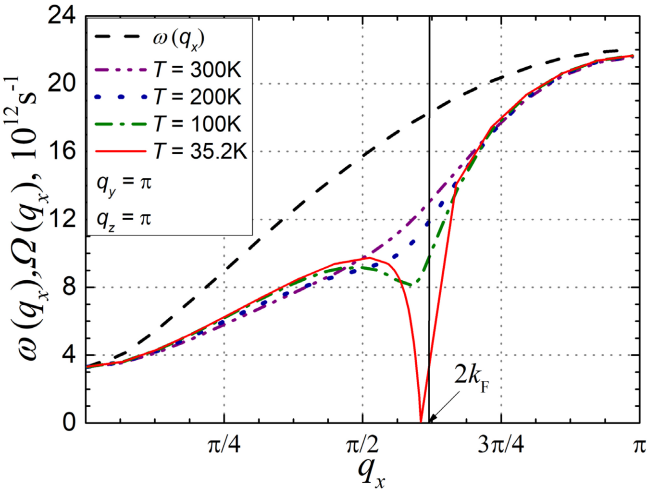

Figure 9. Renormalized phonon spectrum $\Omega(q_x)$ is plotted for various temperatures, with γ_1 = 1.7. The dashed line represents the spectrum of free phonons. Dimensionless Fermi momentum is $k_F = 0.62\pi/2$.

the projections of the phonon quasi-wave vector onto the *x*, *y* and *z* axes, respectively. The initial phonon frequency is denoted as $\omega(q_x)$, and k_F is the Fermi dimensionless quasi-momentum, determined by the carrier concentration variation. Across all figures, it is evident that the values of $\Omega(q_x)$, are reduced compared to the frequency $\omega(q_x)$ in the absence of electron-phonon interaction. This reduction indicates that the electron-phonon interaction diminishes the values of lattice elastic constants. Furthermore, as temperature T decreases, the curves exhibit a change in shape. In the dependencies $\Omega(q_x)$ a minimum appears, becoming more pronounced at lower temperatures. It was anticipated that at a specific temperature, $\Omega(q_x)$ would reach zero for $q_x = 2k_F$, signaling the structural Peierls transition. However, our calculations reveal that renormalized

phonon frequencies reach zero for a value of $q_x \neq 2k_F$. This deviation from $q_x = 2k_F$ is attributed to the deviation of k_F from π/4.

Figure 6 displays the phonon spectrum when $q_y = 0$, $q_z = 0$ and $k_F = 0.56\pi/2$, omitting the interaction between TCNQ chains. In this scenario, the Peierls structural transition occurs solely within TCNQ chains at $T = 90$ K, as experimentally confirmed by a substantial reduction in electrical conductivity. The crystal lattice undergoes a transformation from the initial state with lattice constant b along TCNQ chains to a new crystalline state with constant $4b$. At this temperature, a metal-dielectric phase transition occurs, accompanied by the complete opening of a gap in the carrier spectrum just above the Fermi energy.

When considering the interaction between TCNQ chains (with $q_y \neq 0$, $q_z \neq 0$), the Peierls critical temperature experiences a reduction. Figures 7-9 depict a three-dimensional physical model with $q_y \neq 0$ and $q_z \neq 0$. These figures illustrate the dependencies of $\Omega(q_x)$ on q_x for $q_y = \pi$, $q_z = \pi$, at different values of carrier concentration and temperatures. In Figure 7, where the Fermi momentum $k_F = 0.56\pi/2$, it is noteworthy that $\Omega(q_x)$ reaches zero at $T = 80.9$ K, indicating the occurrence of the transition at this temperature.

Figure 8 shows the renormalized phonon spectrum, $\Omega(q_x)$, for a Fermi momentum of $k_F = 0.59\pi/2$, and with $q_y = \pi$, $q_z = \pi$, taking into consideration the interaction between TCNQ chains. As a consequence, the Peierls transition manifests at $T = 56.9$ K. Notably, it is evident that as carrier concentration increases, the Peierls critical temperature experiences a more pronounced decrease.

In Figure 9, the same dependencies of the renormalized phonon spectrum $\Omega(q_x)$ are presented as in the preceding figures. However, the Fermi momentum is now increased to $k_F = 0.62\pi/2$, with $q_y = \pi$ and $q_z = \pi$ remaining constant. Various temperatures are illustrated in this figure. Notably, the transition temperature continues to decrease, reaching $T = 35.2$ K. This observation underscores that with an increase in carrier concentration, the Peierls critical temperature continues to diminish.

4. Conclusion

The purification and optimization of carrier concentrations demonstrate that crystals of n-type $TTT(TCNQ)_2$ hold significant promise as materials for thermoelectric applications. In $TTT(TCNQ)_2$ the carrier concentration must be increased. It is possible by additional doping with donors and further purification of the crystal. Values of ZT near unity are expected for crystals with $\sigma \approx 2.4 \times 10^4$ $\Omega^{-1}\cdot cm^{-1}$. Detailed modeling of the Peierls transition in $TTT(TCNQ)_2$ crystals in a 3D physical model is presented. We have carried out investigations using a comprehensive physical model of the crystal, that incorporates two most significant electron-phonon interactions. The dispersion of renormalized phonons is calculated in the random phase approximation. Numerical computations of the renormalized phonon spectrum, $\Omega(q_x)$, were conducted across various temperatures and with different values of q_y and q_z. Our findings reveal that neglecting

the interaction between TCNQ chains (q_y = 0 and q_z = 0), initiates the Peierls transition within the TCNQ chains alone, occurring at T = 90 K. However, when considering interchain interaction (q_y = π and q_z = π), the transition completes at a lower temperature of T = 80.9 K. Additionally, our calculations show a notable reduction in the Peierls critical temperature with an increase in carrier concentration. Specifically, for k_F = 0.59π/2, the transition takes place at T = 56.9 K, and for k_F = 0.62π/2, the transition occurs at an even lower temperature of T = 35.2 K. It's crucial to note that these results are obtained under the consideration of interchain interaction. Furthermore, the electron-phonon interaction is observed to reduce the renormalized phonon spectrum, $\Omega(q_x)$, compared to the initial frequency $\omega(q_x)$.

Acknowledgements

The authors express gratitude to the support from the scientific program under the project 20.80009.5007.08 "Study of optoelectronic structures and thermoelectric devices with high efficiency".

Conflicts of Interest

The authors declare no conflicts of interest regarding the publication of this paper.

References

[1] Venkatasubramanian, R., Sivola, E., Colpitts, T. and O'Quinn, B. (2001) Thin-Film Thermoelectric Devices with High Room-Temperature Figure of Merit. *Nature*, **413**, 597-602. https://doi.org/10.1038/35098012

[2] Dresselhaus, M.S. and Heremans, J.P. (2006) Thermoelectric Handbook: Macro to Nano. CRC Press, Boca Raton.

[3] Vining, C.B. (2007) ZT~3.5: Fifteen Years Progress and Things to Come. *The Proceedings of the* 5*th European Conference on Thermoelectrics*, Eindhoven, 18-22 May 2008, 5-10.

[4] Harman, T.C., Walsh, M.P., Laforge, B.E. and Turner, G.W. (2005) Nanostructured Thermoelectric Materials. *Journal of Electronic Materials*, **34**, L19-L22. https://doi.org/10.1007/s11664-005-0083-8

[5] Marlow Inc., "Transmission Lasers (DWDM)", as Accessed on the Website: http://www.marlow.com/industries/telecommunications/transmission-lasers-dwdm.html

[6] Gentherm, "Climate Seats". https://gentherm.com/en/

[7] "Koolatron". https://www.koolatron.com/

[8] d'Angelo, M., Galassi, C. and Lecis, N. (2023) Thermoelectric Materials and Applications: A Review. *Energies*, **16**, Article 6409. https://doi.org/10.3390/en16176409

[9] He, R., Schierning, G. and Nielsch, K. (2018) Thermoelectric Devices: A Review of Devices, Architectures, and Contact Optimization. *Advanced Materials Technologies*, **3**, Article ID: 1700256. https://doi.org/10.1002/admt.201700256

[10] Siouane, S., Jovanovic, S. and Poure, P. (2017) Fully Electrical Modeling of Thermoelectric Generators with Contact Thermal Resistance under Different Operating

Conditions. *Journal of Electronic Materials*, **46**, 40-50. https://doi.org/10.1007/s11664-016-4930-6

[11] Shi, Y., Sturm, C. and Kleinke, H. (2019) Chalcogenides as Thermoelectric Materials. *Journal of Solid State Chemistry*, **270**, 273-279. https://doi.org/10.1016/j.jssc.2018.10.049

[12] Kim, G.H., Shao, L., Zhang, K. and Pipe, K.P. (2013) Engineered Doping of Organic Semiconductors for Enhanced Thermoelectric Efficiency. *Nature Materials*, **12**, 719-723. https://doi.org/10.1038/nmat3635

[13] Sun, Y.M., Sheng, P., Di, C.A., Jiao, F., Xu, W., Qiu, D. and Zhu, D. (2012) Organic Thermoelectric Materials and Devices Based on p- and n-Type Poly (Metal 1, 1, 2, 2-Ethenetetrathiolate)s. *Advanced Materials*, **24**, 932-937. https://doi.org/10.1002/adma.201104305

[14] Taroni, J., Hoces I., Stingelin, N., Heeney, M. and Bilotti, E. (2014) Thermoelectric Materials: A Brief Historical Survey from Metal Junctions and Inorganic Semiconductors to Organic Polymers. *Israel Journal of Chemistry*, **54**, 534-552. https://doi.org/10.1002/ijch.201400037

[15] Casian, A., Pflaum, J. and Sanduleac, I. (2015) Prospects of Low Dimensional Organic Materials for Thermoelectric Applications. *Journal of Thermoelectricity*, **1**, 16-26.

[16] Sanduleac, I. and Casian, A. (2015) Nanostructured TTT$(TCNQ)_2$ Organic Crystals as Promising Thermoelectric n-Type Materials: 3D Modeling. *Journal of Electronic Materials*, **45**, 1316-1320. https://doi.org/10.1007/s11664-015-4018-8

[17] Buravov, L., Eremenko, O., Lyubovskii, R. and Yagubskii, E. (1974) Structure and Electromagnetic Properties of a New High Conductivity Complex $(TTT)^{+}(TCNQ)^{-}_{2}$. *JETP Letters*, **20**, 208-209.

[18] Bulaevskii, L.N. (1975) Peierls Structure Transition in Quasi-One-Dimensional Crystals. *Soviet Physics Uspekhi*, **18**, 131-150. https://doi.org/10.1070/PU1975v018n02ABEH001950

[19] Hohenadler, M., Fehske, H. and Assaad, F.F. (2011) Dynamic Charge Correlations near the Peierls Transition. *Physical Review B*, **83**, Article ID: 115105. https://doi.org/10.1103/PhysRevB.83.115105

[20] Andronic, S. and Casian, A. (2016) Phonons near Peierls Structural Transition in Quasi-One-Dimensional Organic Crystals of TTF-TCNQ. *Advances in Materials Physics and Chemistry*, **6**, 98-104. https://doi.org/10.4236/ampc.2016.64010

[21] Andronic, S. and Casian, A. (2020) Peierls Structural Transition in Q1D Organic Crystals of TTT2I3 for Different Values of Carrier Concentration. *Advances in Materials Physics and Chemistry*, **10**, 239-251. https://doi.org/10.4236/ampc.2020.1010018